JACS
JOURNAL OF THE AMERICAN CHEMICAL SOCIETY
Article
pubs.acs.org/JACS

Alkyne-Tag Raman Imaging for Visualization of Mobile Small Molecules in Live Cells

Hiroyuki Yamakoshi,[†,‡] Kosuke Dodo,[†,‡] Almar Palonpon,[†,§] Jun Ando,[†,‡] Katsumasa Fujita,[†,§] Satoshi Kawata,[§,‡] and Mikiko Sodeoka*[,†,‡]

[†]Sodeoka Live Cell Chemistry Project, Exploratory Research for Advanced Technology, Japan Science and Technology Agency, 2-1 Hirosawa, Wako-shi, Saitama 351-0198, Japan

[‡]RIKEN Advanced Science Institute, 2-1 Hirosawa, Wako-shi, Saitama 351-0198, Japan

[§]Department of Applied Physics, Osaka University, 2-1 Yamadaoka, Suita, Osaka, 565-0871, Japan

Supporting Information

ABSTRACT: Alkyne has a unique Raman band that does not overlap with Raman scattering from any endogenous molecule in live cells. Here, we show that alkyne-tag Raman imaging (ATRI) is a promising approach for visualizing nonimmobilized small molecules in live cells. An examination of structure−Raman shift/intensity relationships revealed that alkynes conjugated to an aromatic ring and/or to a second alkyne (conjugated diynes) have strong Raman signals in the cellular silent region and can be excellent tags. Using these design guidelines, we synthesized and imaged a series of alkyne-tagged coenzyme Q (CoQ) analogues in live cells. Cellular concentrations of diyne-tagged CoQ analogues could be semiquantitatively estimated. Finally, simultaneous imaging of two small molecules, 5-ethynyl-2′-deoxyuridine (EdU) and a CoQ analogue, with distinct Raman tags was demonstrated.

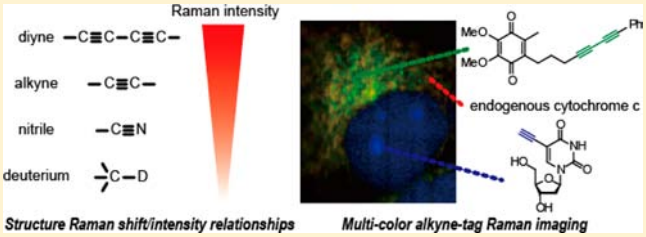

INTRODUCTION

Imaging of molecules in live cells is an important tool in biology, chemical biology, and pharmaceutical and medical sciences. In particular, the use of fluorescent labels has made possible the sensitive detection of specific molecules in living cells. For example, green fluorescent protein (GFP) and related proteins have been widely used as labels for imaging various proteins. However, the use of fluorescent tags is problematic for bioactive small molecules, because sensitive fluorescent dyes, such as derivatives of fluorescein, 4,4-difluoro-4-bora-3a,4a-diaza-*s*-indacene (BODIPY), and many others, have a molecular weight comparable to or even larger than the parent small molecules (Figure 1a). Consequently, fluorescent tags may alter the biological activity, cellular localization, and dynamics of the parent small molecules.[1] To address this issue, click chemistry has recently been employed to introduce a bioorthogonal azide or alkynyl group as a tag. However, a fluorescent group is usually introduced after fixation of the cells for detection of the bioorthogonal tag.

On the other hand, Raman microscopy can visualize the localization of molecules without a fluorescent tag because of its ability to detect molecular vibrations.[2] Recent developments in Raman microscopes have made it possible to obtain high-contrast Raman images of live cells in a reasonable time. But the observable molecular species have been limited to those species existing in large amounts in cells, such as proteins and lipids. Raman signals from small molecules tend to be weak and may easily be masked by intense overlapping Raman signals from dominant intracellular species. However, the alkyne moiety shows a distinct, strong Raman scattering peak in a cellular silent region (1800−2800 cm^{-1}), where most endogenous molecules show no Raman scattering. Thus, alkyne can be used as a tag to image target molecules by Raman microscopy. Focusing on this idea, we developed alkyne-tag Raman imaging (ATRI), which is expected to be applicable to a wide range of molecules. As a proof of concept, we successfully imaged an alkyne-tagged cell proliferation probe, EdU (5-ethynyl-2′-deoxyuridine), in live cells by Raman microscopy[3] (Figure 1b). EdU was covalently incorporated into DNA as a mimic of thymidine, and its localization in the nucleus was clearly visualized. We considered that ATRI should be available for imaging a wide range of mobile noncovalent-bond-forming small molecules, such as specific lipids and drug candidate molecules, in live cells, as well as for estimation of the cellular concentration of such molecules and for multicolor imaging of small molecules in live cells. For these purposes, a basic knowledge of the relationship between structure and Raman shift/intensity of alkynes is essential.

In this paper, we first describe an examination of the structure−Raman shift/intensity relationship of various alkynes. On the basis of these results, we propose guidelines for designing appropriate alkyne-tagged molecules for ATRI. Furthermore, we discuss other candidate small Raman tags

Received: August 31, 2012
Published: December 1, 2012

dx.doi.org/10.1021/ja308529n | J. Am. Chem. Soc. 2012, 134, 20681−20689

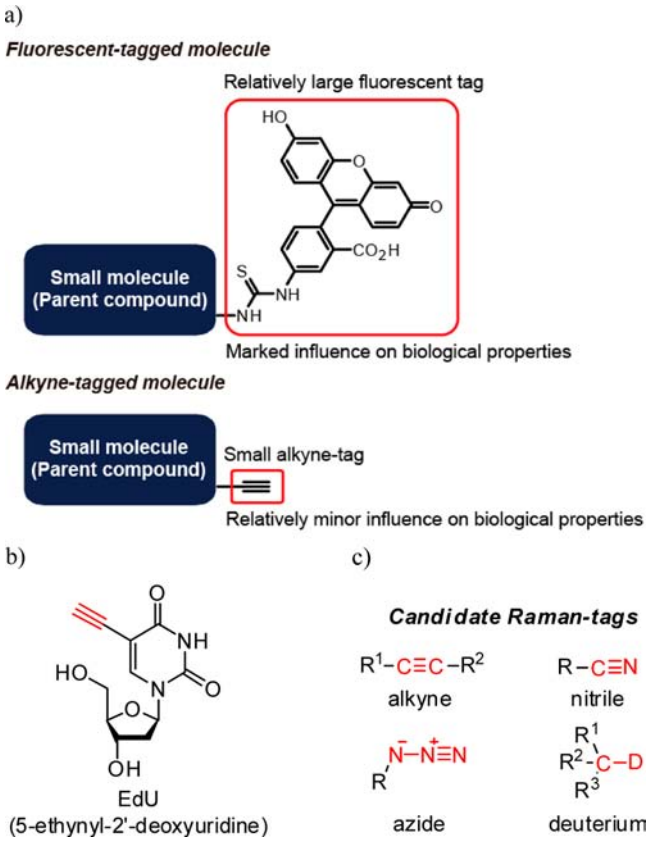

Figure 1. Alkyne tag for specific detection of small molecules by ATRI (alkyne-tag Raman imaging). (a) Comparison of fluorescent tag and alkyne tag. (b) Structure of EdU. (c) Possible bioorthogonal functional groups showing a Raman peak in the cellular silent region.

that exhibit Raman peaks in the cellular silent region (Figure 1c). Using the proposed design guidelines for alkyne tags, we synthesized a series of mobile small-molecular alkyne-tagged coenzyme Q (CoQ) analogues and examined their spatial localization in live cells by Raman microscopy. By calibrating the alkyne Raman intensity with concentration, the cellular concentration of the alkyne-tagged CoQ analogues was semiquantitatively estimated.

Finally, simultaneous multicolor imaging of two small molecules, EdU and a CoQ analogue, with distinct alkyne tags was demonstrated. Our results indicate that ATRI would be a valuable tool for the experimental study of a wide range of small molecules in living cells.

EXPERIMENTAL SECTION

Cell Culture. HeLa human cervical cancer cell line was cultured in Dulbecco's modified Eagle's medium (DMEM) supplemented with 10% fetal bovine serum (FBS) and antibiotics (penicillin/streptomycin).

Reagents. EdU (5-ethynyl-2′-deoxyuridine) was purchased from Invitrogen.

Raman Spectra of Compounds. Raman spectra of compounds were obtained on a slit-scanning Raman microscope (RAMAN-11; Nanophoton, Osaka, Japan) with excitation at 532 or 660 nm. Samples were installed on a glass-bottomed dish (Matsunami, multiwell glass-bottomed dish no. 1S). The laser output was focused into the sample by a 60×/1.2 numerical aperture (NA) water immersion objective lens (UPLSAPO 60XW, Olympus, Tokyo, Japan). The slit width of the spectrograph was 50 μm. The light intensity at the sample plane was 3 mW/μm^2 for 532 nm and 0.3 mW/μm^2 for 660 nm.

Raman Imaging. Raman imaging experiments were performed on a slit-scanning Raman microscope built in our laboratory. Basically, we modified an inverted Nikon Eclipse microscope (TE2000-U, Nikon, Tokyo, Japan) and introduced slit-scanning excitation and detection optics. A 532 nm laser (Verdi V-18, Coherent, Santa Clara, CA) was used for excitation. The laser beam was shaped into a line by a series of cylindrical lenses and focused into the sample by a 60×/1.2 NA water-immersion objective lens (UPLSAPO 60XW, Olympus, Tokyo, Japan). The backscattered Raman signals from the illuminated line were collected by the same objective lens, passed through several Raman edge filters (Semrock, Rochester, NY) and imaged at the entrance slit of a dispersive spectrograph (Bunkoh Keiki, MK-300, Tokyo, Japan). The Raman signals were then dispersed by a grating and detected with a cooled charge-coupled device (CCD) camera (Pixis 400, Princeton Instruments, Trenton, NJ) to obtain the Raman spectra (600−3000 cm^{-1}) simultaneously from multiple points in the line.

To acquire a Raman image, the laser line was scanned in one direction across the sample by use of a single-axis galvano mirror (GSI Lumonics, Billerica, MA) with a step size of ∼0.33 μm, which is larger than the lateral resolution (0.27 μm) of our setup. The slit width of the spectrograph was 40 μm. The laser intensity at the sample plane and exposure time of each line are indicated in the figure captions. The laser intensity was calculated by obtaining the ratio of the measured laser power at the sample position and the area of the illumination line (width = 0.61λ/NA, length was measured from the bright-field image). All reported image acquisition times take into account the spectral data transfer rate of the CCD camera to the PC, which is about ∼3 s/line.

All Raman hyperspectral data sets were postprocessed using the singular value decomposition (SVD) technique for noise reduction and a modified polyfit fluorescence technique for removal of the autofluorescence baseline signal. Finally, the Raman image was constructed by displaying the Raman intensity of the vibrational band of interest at each spatial position. All data processing was performed by in-house image processing software. To remove any nonresonant Raman contributions to the alkyne images, we subtracted the Raman image at a neighboring nonresonant wavenumber from the Raman image at the alkyne peak position.

All cell samples were grown on a quartz substrate. Loading concentration of the Raman-tagged molecules and incubation times are indicated in the figure captions. Prior to Raman imaging, the medium of the cell sample was replaced with a *N*-(2-hydroxyethyl)-piperazine-*N*′-ethanesulfonic acid (HEPES) buffered Tyrode solution composed of NaCl (150 mM), glucose (10 mM), HEPES (10 mM), KCl (4.0 mM), $MgCl_2$ (1.0 mM), $CaCl_2$ (1.0 mM), and NaOH (4.0 mM).

Other Methods. Experimental procedures for chemical synthesis and compound data, including NMR spectra, are given in the Supporting Information.

RESULTS

Relative Raman Intensities of Various Alkynes. To design optimum tag molecules for ATRI, it is indispensable to know the Raman shift and intensity characteristics of various types of alkynes. Although there has been great progress in theoretical studies of Raman spectroscopy, quantitative data on Raman intensities of various alkyne-containing molecules are still very limited, partly because absolute Raman intensities are not easy to measure,[4] and the signal intensity from the same molecule can change depending on the measurement conditions and instrument.[5] Therefore, measurement of relative intensities with respect to a standard molecule under the same conditions is generally used for comparing Raman intensities between different molecules. In the 1960s, Alaune et al.[6] examined the Raman intensities of several alkynes using carbon tetrachloride as an internal standard. Since our aim is imaging of bioactive compounds in live cells, a method to measure the relative Raman intensity of very small amounts of target

dx.doi.org/10.1021/ja308529n | J. Am. Chem. Soc. 2012, 134, 20681−20689

a)

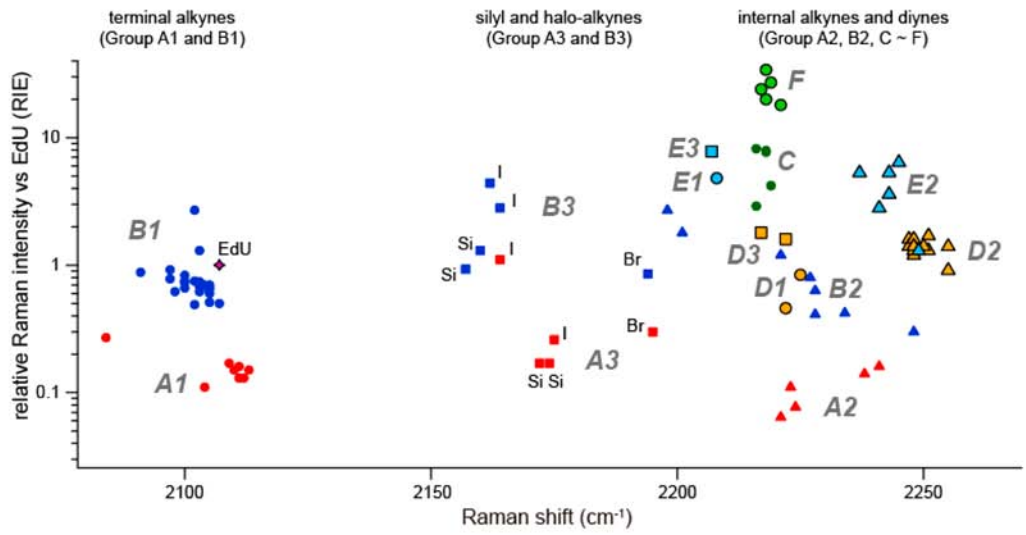

b)

Group	(R: alkyl, alkenyl, acyl etc. / Ar: aryl, X: $SiMe_3$, Br, or I)	number of compounds	average RIE	Raman shift (cm^{-1})	representative example	RIE	Raman shift (cm^{-1})
A1	R—≡—H	8	0.16	2084 ~ 2113	HO—	0.16	2111
A2	R—≡—R	5	0.11	2221 ~ 2241	HO—≡—$(CH_2)CH_3$	0.11	2223
A3	R—≡—X	5	0.40	2164 ~ 2195	HO—≡—$SiMe_3$	0.17	2172
B1	Ar—≡—H	22	0.81	2091 ~ 2107	Ph—≡	0.49	2102
B2	Ar—≡—R	8	1.0	2198 ~ 2248	Ph—≡—$(CH_2)_3CO_2Me$	0.63	2228
B3	Ar—≡—X	5	2.1	2157 ~ 2194	Ph—≡—$SiMe_3$	0.93	2157
C	Ar—≡—Ar	5	6.2	2216 ~ 2219	Ph—≡—Ph	4.2	2219
D1	R—≡—≡—H	2	0.65	2222 ~ 2225	HO—	0.84	2225
D2	R—≡—≡—R	13	1.4	2247 ~ 2255	HO—≡—≡—CMe_3	1.7	2251
D3	R—≡—≡—X	2	1.7	2217 ~ 2222	HO—≡—≡—$SiMe_3$	1.6	2222
E1	Ar—≡—≡—H	1	4.8	2208	Ph—≡—≡	4.8	2208
E2	Ar—≡—≡—R	6	4.1	2237 ~ 2249	Ph—≡—≡—CMe_3	5.3	2237
E3	Ar—≡—≡—X	1	7.8	2207	Ph—≡—≡—$SiMe_3$	7.8	2207
F	Ar—≡—≡—Ar	5	25	2217 ~ 2221	Ph—≡—≡—Ph	27	2219

Other examples of B1 and B3

RIE / Raman shift (cm^{-1})	0.73 / 2100	1.3 / 2103	0.85 / 2194	2.8 / 2164

Figure 2. Structure–Raman shift/intensity relationship of alkynes. (a) Plot of relative Raman intensity versus EdU (RIE) and Raman shift of various types of alkynes. (b) Alkynes are divided into 14 groups according to the substitution pattern. Average RIE, range of Raman shift, and representative alkynes of each group are shown.

molecules is needed. In this study, we employed a simple method for evaluating relative Raman intensity by use of a Raman microscope instead of a normal Raman spectrophotometer. EdU was used as a standard because it has already been used in live cell imaging,[3] and it is chemically stable and nonvolatile. Briefly, the Raman spectrum of a mixture of test compound and EdU in dimethyl sulfoxide (DMSO) was measured, and the relative Raman intensity versus EdU (RIE) was calculated from the intensity of the two alkyne peaks and the molar ratio of the molecules (Figure S1, Supporting Information). Although DMSO shows multiple peaks in the Raman spectrum, none of them appear in the cellular silent region. DMSO is commonly used for preparing stock solutions of bioactive molecules, so it would be convenient if stock solutions could be used directly for this measurement.

By using the above method, Raman shifts and relative Raman intensities of 89 alkynes were evaluated. Figure 2 summarizes the results (for details, see Tables S1–S6 in Supporting Information). Alkynes were divided into 14 groups based on the pattern of substituents, and the data were plotted in a matrix of RIE and Raman shift. The results indicated that conjugation of alkyne to an aromatic ring greatly increases the Raman intensity of the alkyne (RIE, group A < B < C), which is in agreement with previous reports.[6] In addition, the type and position of the substituent in the aromatic ring of π-conjugated groups, such as phenyl and carbonyl groups, influenced the

dx.doi.org/10.1021/ja308529n | J. Am. Chem. Soc. 2012, 134, 20681–20689

alkyne intensity. For example, the RIE of 4-ethynylbenzaldehyde is clearly greater than that of 2-ethynylbenzaldehyde, though the only difference is the position of the formyl group. Formyl and ester substituents at the 4-position of the phenyl group resulted in enhanced intensity, which suggests the importance of extension of π-orbitals in the direction of alkyne stretching (Table S2, Supporting Information). It is noteworthy that iodoacetylene derivatives also showed much higher intensity [(iodoethynyl)benzene vs (bromoethynyl)benzene]. Besides the Raman intensity, Raman shift also varied greatly depending on the substitution pattern. The Raman shifts of terminal alkynes (groups A1 and B1) were generally observed at lower wavenumbers (2080−2120 cm^{-1}). On the other hand, those of internal alkynes (groups A2, B2, and C) were observed at higher wavenumbers (2200 cm^{-1} and higher). Notably, the Raman peaks of trimethylsilyl- or halogen-substituted alkynes appeared between 2150 and 2200 cm^{-1} (groups A3 and B3). The Raman shifts of trimethylsilyl and iodide were observed at 2150−2180 cm^{-1}, whereas that of bromide was near 2200 cm^{-1}.

We also investigated conjugated diynes, butadiynes, as potential Raman tags for ATRI. Interestingly, conjugated diynes (groups D−F) showed much higher intensity (approximately 5 times greater) and higher wavenumbers (2200 cm^{-1} <) compared to simple alkynes (groups A vs D, B vs E, and C vs F). As expected, conjugation of the diyne to an aromatic ring resulted in enhanced intensity (RIE, group D < E < F). Bisaryl-substituted diynes (group F) were found to show the greatest RIE, being about 25 times more intense than EdU on average. Raman shift of these diynes also varied depending on the substitution pattern. Although the peaks of the bisaryl-substituted diynes (group F) appeared at similar wavenumbers (2210−2220 cm^{-1}) to those of the bisaryl-substituted alkynes (group C), peaks of the other types of diynes (groups D and E) appeared at higher wavenumbers compared to those of the simple alkynes (groups A and B).

The results of the evaluation of Raman shifts and Raman intensities of different alkynes enabled us to develop guidelines for designing alkyne-tagged molecules for ATRI. The introduction of the smallest ethynyl group at an appropriate position in the aromatic ring would be a good choice for aromatic compounds. On the other hand, diyne would be a suitable sensitive tag for nonaromatic compounds such as lipids. Diyne may not be a common functional group, but it can easily be prepared from terminal alkyne by cross-coupling reaction (see Supporting Information).[7] Simple two-carbon elongation can afford a 5 times stronger Raman signal. We anticipated that probes with small alkyne tags designed according to these guidelines would be likely to retain the biological activity of the parent molecule and, at the same time, have a sufficiently strong Raman intensity to be detectable with currently available Raman microscopes.

In addition to the alkynyl group, other functional groups, such as nitrile, azide, and deuterium, are expected to show Raman scattering in the cellular silent region (Figure 1c). Nitrile seems to be a promising candidate as a tag because the nitrile group is small and is often used in medicinal chemistry.[8] Azide is also an attractive functional group because it is widely used as a tag for click chemistry. Deuterium is expected to be a good Raman tag because of its small size and limited effects on biological activities. Indeed, Raman imaging of fully deuterated fatty acids has already been reported.[9] We compared these groups on the same scaffold to answer the question "Is alkyne the best tag?" To this end, alkyne-, nitrile-, and azide-tagged hexanoic acids were synthesized and their Raman intensities were compared with that of commercial hexanoic acid-d_{11} (Figure 3a; Scheme S1, Supporting Information). Figure 3a shows the RIE and Raman shifts of the tagged hexanoic acids. As expected, all the tags showed a Raman peak in the cellular silent region (1800−2800 cm^{-1}), indicating their potential value as Raman tags. Compared with alkyne-tagged hexanoic acid, the RIE of nitrile-tagged hexanoic acid was slightly less than half, whereas the RIE of azide-tagged hexanoic acid was quite low. In contrast, hexanoic acid-d_{11} produced multiple signals that overlapped with the EdU peak, and hence evaluation of its RIE was difficult (Raman spectra of tagged hexanoic acids in DMSO are shown in Figure S2 in Supporting Information). Furthermore, we compared the Raman signal of tagged hexanoic acids in a mixture with nitrile as a benchmark, because the Raman shift of nitrile was easy to differentiate among the tags (Figure 3b). The results accord well with the

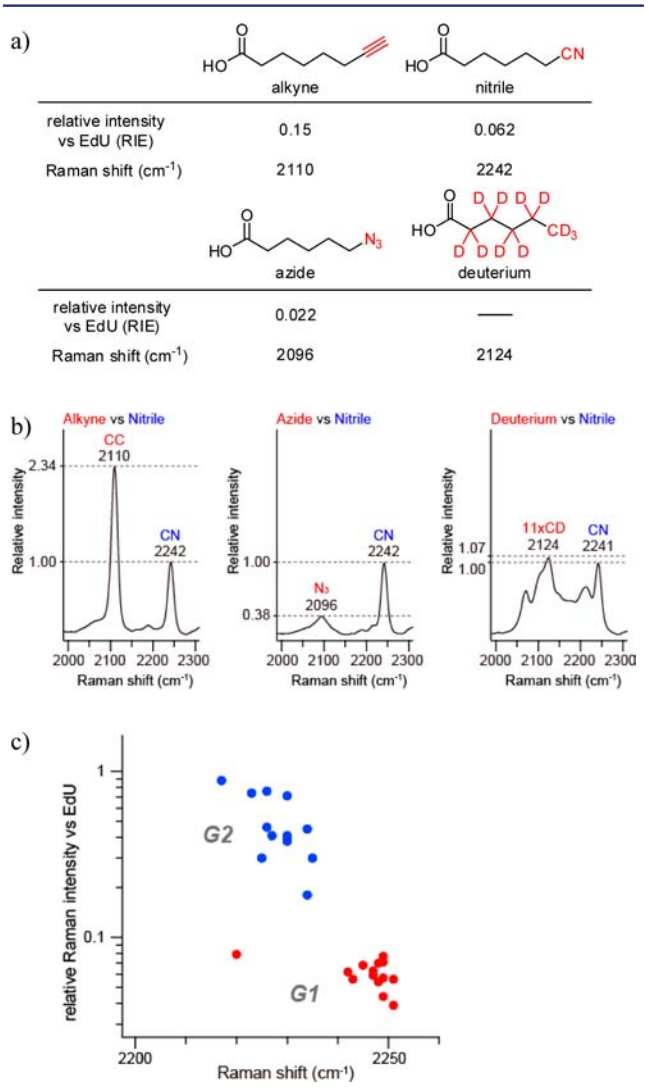

Figure 3. Alkyne is the best tag among the candidate groups. (a) Relative Raman intensities and Raman shifts of tagged hexanoic acids. (b) Comparison of Raman intensity at 500 mM after equal amounts of two hexanoic acid derivatives were mixed in DMSO. (c) Structure−Raman shift/intensity relationship of nitriles. G1, aliphatic nitriles; G2, aromatic nitriles.

dx.doi.org/10.1021/ja308529n | J. Am. Chem. Soc. 2012, 134, 20681−20689

RIE values. To further examine the relative intensity of deuterium, the Raman spectrum of acetonitrile-d_3 was measured (Figure S3, Supporting Information). The Raman intensity derived from the three identical C−D bonds was comparable with that of nitrile. The small size and relatively high Raman intensity of deuterium appear promising, but the complexity of the signal severely limits its potential for multicolor imaging. In view of the above results, we concluded that alkyne tags are the most suitable for Raman imaging among the functional groups evaluated.

Although the Raman intensity of nitrile was lower than that of alkyne, it might still be useful as a Raman tag. Since information about the relative Raman intensity of nitriles is limited,[10] we examined the relative Raman intensities of 28 nitriles (Figure 3c; Table S7, Supporting Information). As was the case with alkyne, conjugation to an aromatic ring amplified the intensity (group G1 < G2). Nevertheless, the intensity of the nitrile signal was generally weaker than that of the corresponding terminal alkyne (groups A1 vs G1 and B1vs G2) (Figure S4, Supporting Information).

Overall, not only alkyne but also nitrile and deuterium appear to be suitable for use as Raman tags, but among them, alkyne has clear advantages in terms of high signal intensity, narrow line width, and suitable wavenumber of the signal.

Alkyne-Tag Raman Imaging of Coenzyme Q Analogues. With these basic structure−Raman intensity relationships in hand, we set out to test the validity of our approach for the live cell imaging of mobile small molecules, focusing on lipids as typical mobile molecules that are not immobilized under normal fixation conditions.[11] In particular, we are interested in the mitochondrial lipid CoQ, which is an essential and abundant molecule in cells, functioning as an electron transporter in the mitochondrial respiratory chain and an endogenous antioxidant.[12] Because endogenous CoQ species, such as CoQ_{10}, are too hydrophobic to be incorporated into cells exogenously, many low-molecular-weight analogues, such as decylubiquinone and idebenone, have been developed and investigated.[13] In many cases, the length of the side chain affects the biological activity, indicating that their cellular uptake and accumulation might be dependent upon their hydrophobicity.[14] Nevertheless, information about cellular uptake of CoQ analogues is quite limited,[15] mainly because of the lack of a quantitative detection method for small molecules in living cells. Therefore, CoQ analogues would be suitable target molecules to demonstrate the value of ATRI.

First, we designed and synthesized several alkyne-tagged CoQ analogues, AltQ1−8, with different types of alkyne tag and appropriate hydrophobicity (i.e., cLogP values similar to those of idebenone and decylubiquinone) (Figure 4a; Scheme S2, Supporting Information). HeLa cells were incubated in the presence of 20 μM AltQs for 1 h, and averaged Raman spectra were obtained by irradiation at 532 nm with scanning at 3 s/line. The averaged Raman spectra obtained from 10 × 10 pixels (3.6 μm × 3.6 μm) in the cytoplasmic regions of 21 living cells and the relative Raman intensity are shown in Figure 4 panels b and c, respectively (averaged Raman spectra of the extracellular region are shown in Figure S5 in Supporting Information). The Raman signals of alkynes with RIE values larger than ca. 0.5 (AltQ1−6) were easily detected in live cells (Figure 4c). Furthermore, we observed a rough correlation between the relative Raman intensity of the AltQs in DMSO and those in cells, except for AltQ1 (Figure 4c). The observed Raman signal of AltQ1 in cells was much weaker than expected from the RIE

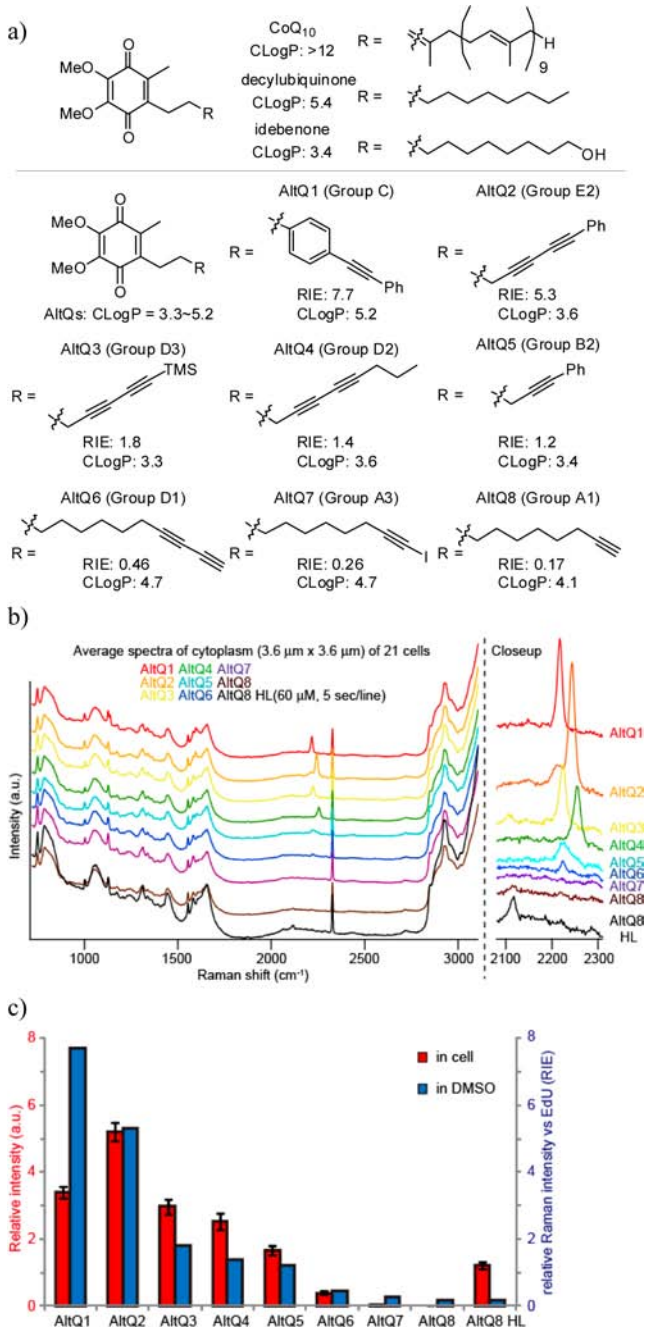

Figure 4. Relative Raman intensity of AltQs in live HeLa cells. (a) Structures and RIE and predicted cLogP values of AltQs. cLogP values were predicted by ChemBioDraw Ultra 12.0. (b) Average Raman spectra of cytoplasmic region (3.6 μm × 3.6 μm) of 21 cells cultured with AltQs. Sample concentration was 20 μM, the light intensity at the sample plane was 3 mW/μm^2, and the exposure time for each line was 3 s with the exception of AltQ8HL (HL = high concentration and long exposure). In the case of AltQ8HL, the sample concentration was 60 μM. The light intensity at the sample plane was 3 mW/μm^2, and the exposure time for each line was 5 s. Spectra are vertically offset for ease of viewing. (c) Relative Raman intensity of AltQs in DMSO and in cells.

value measured in DMSO. This may be due to poor uptake of AltQ1, which has a high cLogP value. This point will be discussed in detail in the next section. The alkyne peak of AltQ8 with a simple terminal alkyne was not observed under these conditions (3 s/line irradiation, 20 μM concentration),

dx.doi.org/10.1021/ja308529n | J. Am. Chem. Soc. 2012, 134, 20681−20689

but the peak was clearly observed when the cells were treated with 60 μM AltQ8 for 1 h and scanned at 5 s/line. Hence, even the weakest-intensity class of alkyne (RIE = 0.17) can still be used as a Raman tag, if it is sufficiently accumulated in cells and scanning conditions are set appropriately. The results obtained with the alkyne-tagged CoQ analogues in cells were consistent with the RIE values obtained in DMSO, validating our guidelines for designing alkyne tags.

After confirming the Raman shifts/intensities of the alkyne-tagged CoQ analogues, we use ATRI to visualize the distribution of CoQ molecules in cells. Endogenous CoQ_{10} is known to exist mainly in mitochondria, where it is synthesized and works as an electron transporter in the respiratory chain. Moreover, the cellular distribution of exogenously added CoQ_{10} was examined by differential centrifugation,[15b] and CoQ_{10} was reported to be enriched mainly in the mitochondrial fraction. These results imply the existence of a molecular mechanism of mitochondrial accumulation of CoQ-related compounds. However, the distribution of short-chain CoQ analogues in living cells has not been studied due to the difficulty in fluorescent labeling of CoQ. Therefore, we attempted Raman imaging of AltQ in live cells. Figure 5 shows Raman imaging of AltQ4 in live HeLa cells as a representative example (see also Figures S6 and S7 in Supporting Information). Live HeLa cells were treated with 6 μM AltQ4, and after 50 min, a Raman image of the cells was obtained with 532 nm excitation.

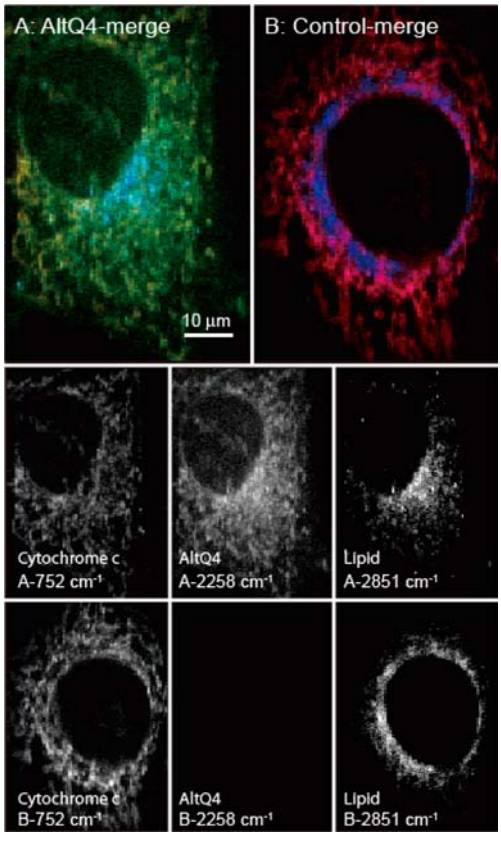

Figure 5. Raman imaging of AltQ4 in living HeLa cells. (A) Raman image obtained from HeLa cells treated with 6 μM AltQ4. Images at 752, 2258, and 2851 cm^{-1} are shown in the lower panels. The overlay images at 752, 2258, and 2851 cm^{-1} (top panels) were assigned to the red, green, and blue channels, respectively. The light intensity at the sample plane was 3 $mW/\mu m^2$. The exposure time for each line was 5 s. The total number of lines of exposure was 95. The image acquisition time was 13 min. (B) Raman image obtained from control HeLa cells under the same conditions.

Images were reconstructed from the distribution of Raman peaks at 752, 2258, and 2851 cm^{-1}, which were assigned to cytochrome *c*, AltQ4 (diyne tag), and lipid molecules (CH_2 stretching), respectively. As is evident in Figure 5, no signal at 2258 cm^{-1} was observed in the nontreated control HeLa cells.[3,16] In contrast, AltQ4-treated cells showed a clear signal at 2258 cm^{-1} due to the alkyne. AltQ4 was colocalized with cytochrome *c* to a considerable extent, indicating that AltQ4 was mainly accumulated in mitochondria. However, the accumulation of AltQ4 seemed not to be specific to mitochondria under these conditions, and it was also colocalized with lipids. This is consistent with the reported distribution of CoQ.[15b] These results confirm that ATRI is a promising tool for studying cellular uptake and accumulation of small molecules.

Estimation of Cellular Concentration of CoQ Analogues. Following the successful imaging of AltQs, we set out to estimate the concentration of AltQs in cells by using Raman microscopy. Cellular accumulation of fluorescence-labeled molecules is expected to be markedly influenced by the fluorescent moiety due to its bulkiness relative to the parent compound. In contrast, a diyne tag (molecular weight 48) is considered to be sufficiently small and may have relatively little influence on the properties of the parent compound. Therefore, the dynamics of cellular accumulation of the tagged compound may well reflect that of the parent compound.

As previously mentioned, the efficiency of cellular uptake of CoQ analogs is believed to be dependent on their cLogP values. To confirm this, we prepared a series of diyne-tagged CoQ analogues, AltQ4 and AltQ9−16, which have side chains of different lengths (C9∼C17) (Figure 6a; Scheme S3, Supporting Information). As expected, the relative Raman intensities of the alkyne in these analogues were similar, whereas the cLogP values increased with increasing length of the side chain.

For the estimation of cellular accumulation, HeLa cells were incubated in the presence of 20 μM diyne-tagged CoQ analogues for 1 h, and averaged Raman spectra were obtained by excitation at 532 nm with scans of 10 s/line. Cellular concentration of diyne-tagged CoQ analogues was derived by measuring the alkyne signal intensity of the averaged Raman spectra from 10 × 10 pixels (3.6 μm × 3.6 μm) in the cytoplasmic regions of 21 living cells and using a calibration curve obtained from the Raman spectra of diyne-tagged CoQ analogues in solution (Figure 6b; Figure S8, Supporting Information).

The cytoplasmic concentration of the shortest analogue, AltQ9, was estimated to be about 2 mM, which is up to 100 times higher than the treatment concentration, indicating efficient uptake and accumulation of this molecule. The estimated cytoplasmic concentrations of the analogues apparently decreased in proportion to the chain length (and cLogP value). These results are in agreement with reported findings that the cellular activity of shorter side chain analogues such as decylubiquinone and idebenone is greater than that of exogenously added superhydrophobic CoQ_{10}.[17] Remarkably, the observed differences in accumulation of CoQ analogues imply that a slight change in the side chain length of CoQ analogues, even a one-carbon difference, greatly affects the efficiency of cellular uptake. Although, as shown in Figure 5, the

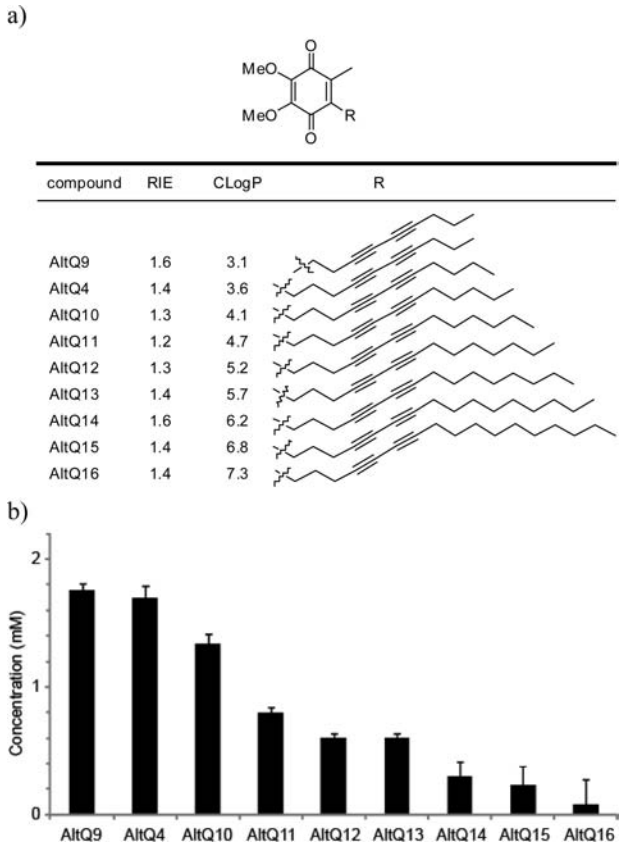

Figure 6. Relative Raman intensity of diyne-tagged analogues in live HeLa cells. (a) Structures and RIE and predicted cLogP values of diyne-tagged analogues. cLogP values were predicted by use of ChemBioDraw Ultra 12.0. (b) Estimation of cellular concentration of AltQs. Averaged Raman spectra of cytoplasmic region (3.6 μm × 3.6 μm) of 21 cells cultured with AltQs were used. Sample concentration was 20 μM. Incubation time was 60 min. The light intensity at the sample plane was 3 mW/μm^2, and the exposure time for each line was 10 s.

distribution of the molecules in cells is not uniform and the calibration curve in DMSO may not accurately reflect the cellular environment, ATRI can nonetheless provide approximate values of concentration. This ability to semiquantitatively estimate cellular accumulation of small molecules represents a major advantage of ATRI.

Two-Color Alkyne-Tag Raman Imaging. Finally, we attempted simultaneous two-color imaging with ATRI. For this purpose, we selected two alkyne-tagged molecules, EdU and AltQ2, which show alkyne signals at different wavenumbers. HeLa cells were treated with 40 μM EdU for 1 day, and then excess EdU was washed out and Raman images of live HeLa cells were obtained in the presence of 2 μM AltQ2 with excitation at 532 nm and scanning at 10 s/line.

Two different alkyne peaks at 2122 and 2248 cm^{-1}, corresponding to EdU and AltQ2, respectively, were easily discriminated (Figure S9, Supporting Information). Raman images reconstructed from the distribution of Raman signals at 2122 and 2248 cm^{-1} clearly indicated different localization patterns of these two molecules (Figure 7). EdU was localized in the nucleus, whereas AltQ2 was localized in the cytoplasm.[18] An advantage of using Raman microscopy is that recording of the Raman spectrum at various regions of interest in the cell is possible. Therefore, multiple Raman peaks derived from

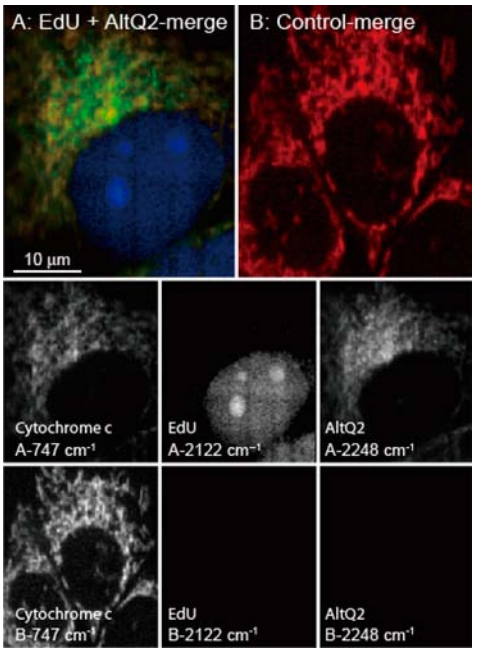

Figure 7. Two-color alkyne-tag Raman imaging. (A) Raman image obtained from HeLa cells treated with 40 μM EdU for 1 day and 2 μM AltQ2 for 30 min. (B) Control HeLa cells. Images at 747, 2122, and 2248 cm^{-1} are shown at the lower panels. The overlay images at 747, 2122, and 2248 cm^{-1} (top panels) were assigned to the blue, red, and green channels, respectively. The light intensity at the sample plane was 3 mW/μm^2. The exposure time for each line was 10 s. The total number of lines of exposure was 170. The image acquisition time was 38 min.

exogenous molecules as well as various endogenous biomolecules such as cytochrome *c* can be detected and imaged simultaneously. In comparison, Raman imaging of control HeLa cells confirmed that the signals at 2122 and 2248 cm^{-1} were derived from alkyne-tagged molecules and that the cytochrome *c* signal was from the endogenous compound. Since we already know the structure−Raman shift relationships of various alkyne molecules, simultaneous multicolor imaging of more than two alkyne-tagged molecules should be possible by selecting appropriate combinations of alkyne tags. This would make ATRI a useful imaging platform for studying interactions of multiple small molecules in cells.

■ DISCUSSION

Our recently developed alkyne-tag Raman imaging (ATRI) method permits visualization of small molecules in living cells by using very small Raman-active tags that lack the disadvantages of larger fluorescent tags, which may markedly influence the chemical and biological properties of the parent molecule.[3] Here, to extend the scope of our method to nonimmobilized small molecules, such as lipids, we first examined the structure−Raman intensity relationships of a series of alkynes to provide a basis for the molecular design of efficient ATRI probes. The results clearly showed the efficacy of both an alkyne moiety conjugated to an aromatic ring and a conjugated diyne. Thus, if the parent compound has an aromatic moiety, the introduction of the small ethynyl group at an appropriate position on the aromatic ring would be an excellent choice and might have relatively little effect on the biological properties. In the case of aliphatic molecules, diyne may be a suitable choice as a tag. Since various synthetic

dx.doi.org/10.1021/ja308529n | J. Am. Chem. Soc. 2012, 134, 20681−20689

methods for alkynes conjugated to an aromatic ring[19] and conjugated diynes[7] are well established, synthesis of appropriately tagged molecules should not present much difficulty (see also Supporting Information).

In this report, the Raman intensities of various alkyne tags were evaluated by use of EdU as standard. In order for other researchers to better evaluate our approach for their own applications, it is useful to compare the Raman intensity of alkyne with typical biological molecules. One such molecule is phenylalanine, an amino acid found in cells that exhibits a strong Raman peak around 1000 cm^{-1}, assigned to the ring breathing mode (Figure 4b).[16b] The Raman intensity of phenylalanine was compared with that of EdU by measuring the Raman spectrum of an equimolar mixture (Figure S11, Supporting Information). Clearly, the EdU signal was about 5 times stronger than the phenylalanine signal. Hence, the Raman intensities of various alkyne tags could be estimated relative to the intensity of the phenylalanine ring breathing mode peak, based on the RIE values reported here.

To evaluate our design strategy for ATRI probes, we performed Raman imaging of a series of CoQ analogues. The relative Raman intensities of CoQ analogues having various alkyne tags in live cells were first compared with the RIE values in DMSO, and the results indicated that RIE in DMSO is a good index for evaluating potential Raman tags. We then used the ATRI method to visualize diyne-tagged AltQ4 in live cells, confirming the utility of ATRI for imaging small mobile molecules. Furthermore, the cellular accumulation of CoQ analogues with different lengths of side chain (diyne-tagged CoQ analogues) was estimated semiquantitatively with ATRI, and the results indicated that uptake of the CoQ analogues is dependent on their cLogP value, as expected. Finally, we successfully demonstrated simultaneous imaging of EdU and AltQ2 in live cells, indicating the potential of ATRI for multicolor imaging. It is important to note that although mammalian cells do not normally contain molecules bearing an alkynyl group, many alkyne-containing natural products have been found, for example, in plants.[20] Also, many pharmaceutical molecules studied in medicinal chemistry contain an alkyne moiety.[21]Therefore, it should be possible to perform Raman imaging of such molecules without any modification.

As an imaging technique, ATRI has several advantages over conventional fluorescence microscopy. Aside from its main advantage of using a very small tag, the alkyne tag signal does not degrade over repeated scans, unlike fluorescent probes, which suffer from photobleaching. Moreover, since a Raman spectrum is obtained at each pixel, ATRI has the ability to delineate many other cellular structures in addition to the alkyne-tagged structures in one scan. On the other hand, the fluorescence technique can only show stained structures. However, in terms of sensitivity and imaging speed, ATRI is a much less sensitive technique than fluorescence imaging. With the current Raman instrument, the sensitivity of Raman detection for alkyne tags approaches the submillimolar range (about 0.1−0.2 mM for the more intense diynes), whereas recent fluorescence techniques can detect down to a single molecule.[22] Furthermore, image acquisition for ATRI takes several tens of minutes, while video-rate speed is easily achievable for fluorescence imaging.

All the results presented here were obtained by spontaneous Raman imaging microscopy, but the concept of ATRI is also applicable to nonlinear Raman imaging techniques, such as coherent anti-Stokes Raman scattering (CARS)[23] and stimulated Raman scattering (SRS)[24] microscopy. These nonlinear techniques should offer faster image acquisition and greater detection sensitivity.

CONCLUSIONS

In conclusion, we examined the structure−Raman shift/intensity relationship of various alkynes that resulted in guidelines for designing appropriate alkyne tags. With the aid of the obtained relationships, we have achieved live cell imaging of alkyne-tagged CoQ analogues as examples of mobile small molecules and the simultaneous two-color imaging of two small molecules. To our knowledge, this is the first example of direct multicolor imaging of small molecules without fluorescent labels in living cells. We believe there is enormous potential for application of ATRI in biological research in the near future.

ASSOCIATED CONTENT

Supporting Information

Eleven figures, seven tables, three schemes, and additional text showing detailed experimental procedures, characterization of all compounds, and additional experimental results. This material is available free of charge via the Internet at http://pubs.acs.org.

AUTHOR INFORMATION

Corresponding Author

sodeoka@riken.jp

Notes

The authors declare no competing financial interest.

ACKNOWLEDGMENTS

We thank Dr. Minoru Kobayashi of Nanophoton Corporation for helpful discussions. We thank Professor Yoshiharu Iwabuchi for generously providing AZADO. This work was partly supported by a Grant-in-Aid for Young Scientist (B) (23710276 to H.Y.) from the Ministry of Education, Culture, Sports, Science and Technology, Japan.

REFERENCES

(1) (a) Yamakoshi, H.; Ohori, H.; Kudo, C.; Sato, A.; Kanoh, N.; Ishioka, C.; Shibata, H.; Iwabuchi, Y. *Bioorg. Med. Chem.* **2010**, *18*, 1083−1092. (b) Thuaud, F.; Bernard, Y.; Turkeri, G.; Dirr, R.; Aubert, G.; Cresteil, T.; Baguet, A.; Tomasetto, C.; Svitlin, Y.; Sonenberg, N.; Nebigil, C. G.; Désaubry, L. *J. Med. Chem.* **2009**, *52*, 5176−5187.

(2) (a) Puppels, G. J.; Greve, J. *J. Appl. Spectrosc.* **1993**, *47*, 1256−1267. (b) Uzunbajakava, N.; Otto, C. *Opt. Lett.* **2003**, *28*, 2073−2075. (c) Huang, Y.-S.; Karashima, T.; Yamamoto, M.; Hamaguchi, H. *Biochemistry* **2005**, *44*, 10009−10019. (d) Mattäus, C.; Boydston-White, S.; Miljković, M.; Romeo, M.; Diem, M. *Appl. Spectrosc.* **2006**, *60*, 1−8. (e) Fujita, K.; Smith, N. I. *Mol. Cells* **2008**, *26*, 530−535.

(3) Yamakoshi, H.; Dodo, K.; Okada, M.; Ando, J.; Palonpon, A.; Fujita, K.; Kawata, S.; Sodeoka, M. *J. Am. Chem. Soc.* **2011**, *133*, 6102−6105.

(4) Larkin, P. J.; Gustafson, W. G.; Asher, S. A. *J. Chem. Phys.* **1991**, *94*, 5324−5330.

(5) (a) Rea, D. G. *J. Mol. Spectrosc.* **1960**, *4*, 507−517. (b) Binet, C.; Romanet, R. *J. Raman Spectrosc.* **1976**, *5*, 253−267.

(6) (a) Alaune, Z.; Talaikyte, Z. *Liet. TSR Mokslu Akad. Darb., Ser. B* **1967**, 55−66. (b) Alaune, Z.; Talaikyte, Z. *Liet. TSR Mokslu Akad. Darb., Ser. B* **1964**, 57−64. (c) Alaune, Z.; Mozolis, V. *Liet. TSR Mokslu Akad. Darb., Ser. B* **1963**, 101−105.

(7) (a) Yin, W.; He, C.; Chen, M.; Zhang, H.; Lei, A. *Org. Lett.* **2009**, *11*, 709−712. (b) Siemsen, P.; Livingston, R. C.; Diederich, F. *Angew.*

Chem., Int. Ed. **2000**, *39*, 2632−2657. (c) Shun, A. L. K. S.; Tykwinski, R. R. *Angew. Chem., Int. Ed.* **2006**, *45*, 1034−1057.
(8) Jones, L. H.; Summerhill, N. W.; Swain, N. A.; Mills, J. E. *Med. Chem. Commun.* **2010**, *1*, 309−318.
(9) (a) Manen, H.-J.; van, Kraan, Y. M.; Roos, D.; Otto, C. *Proc. Natl. Acad. Sci. U.S.A.* **2005**, *102*, 10159−10164. (b) Xie, X. S.; Yu, J.; Yang, W. Y. *Science* **2006**, *312*, 228−230. (c) Manen, H.-J.; van, Lenferink, A.; Otto, C. *Anal. Chem.* **2008**, *80*, 9576−9582.
(10) (a) Muldakhmetov, Z. M.; Kupriyanov, N. S.; Akhmetkarimov, K.; Mai, I. *Izv. Akad. Nauk Kaz. SSR, Ser. Khim.* **1972**, *22*, 38−72. (b) Krasnomolova, L. P.; Kushnikov, Y. A. *Izv. Akad. Nauk Kaz. SSR, Ser. Khim.* **1967**, *17*, 31−36. (c) Shorygin, P. P.; Geiderikh, M. A.; Ambrush, T. I. *Zh. Fiz. Khim.* **1960**, *34*, 335−342.
(11) Tanaka, K. A. K.; Suzuki, K. G. N.; Shirai, Y. M.; Shibutani, S. T.; Miyahara, M. S. H.; Tsuboi, H.; Yahara, M.; Yoshimura, A.; Mayor, S.; Fujiwara, T. K.; Kusumi, A. *Nat. Methods* **2010**, *7*, 865−866.
(12) (a) Rakita, R. M.; Michael, B. R.; Rosen, H. *Biochemistry* **1989**, *28*, 3031−3036. (b) Bentinger, M.; Tekle, M.; Dallner, G. *Biochem. Biophys. Res. Commun.* **2010**, *396*, 74−79.
(13) (a) Armstrong, J. S.; Whiteman, M.; Rose, P.; Jones, D. P. *J. Biol. Chem.* **2003**, *278*, 19079−49084. (b) Suno, M.; Nagaoka, A. *Jpn. J. Pharmacol.* **1984**, *35*, 196−198. (c) Shimamoto, N.; Goto, N.; Hirata, M. *Nippon Yakurigaku Zasshi (Jpn. J. Pharmacol.)* **1982**, *80*, 137−145.
(14) (a) Helfenbaum, L.; Ngo, A.; Ghelli, A.; Linnane, A. W.; Esposti, M. D. *J. Bioenerg. Biomembr.* **1997**, *29*, 71−80. (b) Esposti, M. D.; Ngo, A.; McMullen, G. L.; Ghelli, A.; Sparla, F.; Benelli, B.; Ratta, M.; Linnane, A. W. *Biochem. J.* **1996**, *313*, 327−334.
(15) (a) Ross, M. F.; Prime, T. A.; Abakumova, I.; James, A. M.; Porteous, C. M.; Smith, R. A.; Murphy, M. P. *Biochem. J.* **2008**, *411*, 633−645. (b) The CoQ accumulating system in mitochondria has not been completely elucidated. Niki and co-workers reported that CoQ10 distribution in PC12 cells exhibited a nonlinear relationship with lipid distribution. In contrast, the distribution of lipophilic antioxidant αT was directly proportional to the lipid distribution. These results suggest that the accumulation of CoQ in mitochondria is mediated by some mitochondrial proteins possessing CoQ-binding properties. See Saito, Y.; Fukuhara, A.; Nishio, K.; Hayakawa, M.; Ogawa, Y.; Sakamoto, H.; Fujii, K.; Yoshida, Y.; Niki, E. *J. Nutr. Biochem.* **2009**, *20*, 350−357.
(16) (a) Okada, M.; Smith, N. I.; Palonpon, A. F.; Endo, H.; Kawata, S.; Sodeoka, M.; Fujita, K. *Proc. Natl. Acad. Sci. U.S.A.* **2012**, *109*, 28−32. (b) Hamada, K.; Fujita, K.; Smith, N. I.; Kobayashi, M.; Inoue, Y.; Kawata, S. *J. Biomed. Opt.* **2008**, *13*, No. 044027. (c) Ando, J., Fujita, K. *Curr. Pharm. Biotechnol.* (in press).
(17) Haefeli, R. H.; Erb, M.; Gemperli, A. C.; Robay, D.; Fruh, I. C.; Anklin, C.; Dallmann, R.; Gueven, N. *PLoS One* **2011**, *6*, No. e17963.
(18) The Raman imaging of EdU distribution reveals higher uptake of EdU in the nucleolus compared to other regions in the nucleus. The nucleolus uptake of EdU was still observed even after fixation and permeabilization of the cell, which is remarkably opposite from the results obtained by click chemistry (Figure S10, Supporting Information). One way to interpret this discrepancy is that the click reactant could not access the nucleolus under the examined conditions or the click reaction did not proceed. Although it is difficult to draw any conclusions from these observations, our Raman images show without doubt that alkyne is present in the nucleolus. This goes to show that ATRI may get to see the blind spots of click chemistry.
(19) (a) Chinchilla, R.; Nájera, C. *Chem. Rev.* **2007**, *107*, 874−922. (b) Doucet, H.; Hierso, J.-C. *Angew. Chem., Int. Ed.* **2007**, *46*, 834−871.
(20) (a) Roman, M.; Dobrowolski, J. C.; Baranska, M.; Baranski, R. *J. Nat. Prod.* **2011**, *74*, 1757−1763. (b) Dembitsky, V. M. *Lipids* **2006**, *41*, 883−924.
(21) (a) Christiansen, E.; Urban, C.; Grundmann, M.; Due-Hansen, M. E.; Hagesaether, E.; Schmidt, J.; Pardo, L.; Ullrich, S.; Kostenis, E.; Kassack, M.; Ulven, T. *J. Med. Chem.* **2011**, *54*, 6691−6703. (b) Crosignani, S.; Prêtre, A.; Jorand-Lebrun, C.; Fraboulet, G.; Seenisamy, J.; Augustine, J. K.; Missotten, M.; Humbert, Y.; Cleva, C.; Abla, N.; Daff, H.; Schott, O.; Schneider, M.; Burgat-Charvillon, F.; Rivron, D.; Hamering, I.; Arrighi, J.-F.; Gaudet, M.; Zimmerli, S. C.; Juillard, P.; Johnson, Z. *J. Med. Chem.* **2011**, *54*, 7299−7317. (c) Knaus, E. E.; Innocenti, A.; Scozzafava, A.; Supuran, C. T. *Bioorg. Med. Chem. Lett.* **2011**, *21*, 5892−5896.
(22) Taniguchi, Y.; Choi, P. J.; Li, G.-W.; Chen, H.; Babu, M.; Hearn, J.; Emili, A.; Xie, X. S. *Science* **2010**, *329*, 533−538.
(23) (a) Zumbusch, A.; Holtom, G. R.; Xie, X. S. *Phys. Rev. Lett.* **1999**, *82*, 4142−4145. (b) Okuno, M.; Kano, H.; Leproux, P.; Couderc, V.; Day, J. P. R.; Bonn, M.; Hamaguchi, H. *Angew. Chem., Int. Ed.* **2010**, *49*, 6773−6777.
(24) (a) Freudiger, C. W.; Min, W.; Saar, B. G.; Lu, S.; Holtom, G. R.; He, C.; Tsai, J. C.; Kang, J. X.; Xie, X. S. *Science* **2008**, *322*, 1857−1861. (b) Saar, B. G.; Freudiger, C. W.; Reichman, J.; Stanley, C. M.; Holtom, G. R.; Xie, X. S. *Science* **2010**, *330*, 1368−1370.